Antenna Pattern Retrieval from Reflection Coefficient Measurements with Reflective Loads

Zhou Du[*]**, Ville Viikari, Juha Ala-Laurinaho, Aleksi Tamminen, and Antti V. Räisänen**

Abstract—This paper presents a new method for antenna pattern retrieval from reflection coefficient measurements. A reflective load with known reflective properties is placed close to the aperture of the antenna under test. The reflection coefficient of the antenna is measured at the antenna feed with multiple different reflective loads. The antenna pattern is then solved from the measurements with an inversion method. This paper derives and verifies the analytical foundations needed to implement the method, and demonstrates the method both by simulations and experiments for a pyramidal horn antenna at 30 GHz.

1. INTRODUCTION

Traditionally the antenna pattern is measured in a far-field, near-field, or compact antenna test range. In the far-field technique, a reference antenna is placed in the far-field of the antenna under test (AUT). The transmission between the AUT and the reference antenna is then recorded at different rotations of the AUT. In the near-field measurement technique, the near-field of the AUT is sampled spatially with a suitable probe antenna moving over the measurement surface. The measured near-field distribution is then used to calculate the antenna far-field radiation properties. The compact range is suitable for electrically large antennas, whose far-field distance is too large to accommodate the range in an anechoic chamber. Typically the distance is defined as $2D^2/\lambda$, where D is the largest dimension of the antenna aperture and λ is the wavelength. In the compact antenna range, planar wavefront representing far-field conditions is generated with a collimating element, such as a reflector or a lens. At high frequencies, the planar wavefront may also be convenient to be generated with a radio hologram [1–3].

There are certain limitations to the traditional methods. First, in any method, one antenna is either moved or rotated during the measurement. Antennas are connected to the measurement equipment with cables that, when moved or rotated, easily change their properties, such as the electrical length. At high frequencies, even a small relative change in the dimensions of the cable may cause a huge phase change to the transmitted signal, because the cable can be electrically very long. Although the error compensation techniques have been introduced [4], the measurement errors due to bending cables may be significant especially in the planar near-field scanning at high frequencies. Another limitation with far-field and compact ranges is that they require a relatively large space.

The aforementioned methods require a cable connection to the AUT. Some antennas, such as RFID antennas, are typically attached directly to an RFID chip and there is no possibility for a cable connection. Then, antenna radar cross section (RCS) measurement technique can be used to characterize the antenna [5–8]. In the RCS measurement technique, a modulating load, such as the RFID chip is attached to the AUT. The AUT is illuminated with a continuous wave and modulated backscattered signal is measured as a function of the antenna orientation. This method avoids the problems related

to flexing cables, but it requires a potentially large far-field antenna range. In addition, the method suffers from reduced dynamic range due to the two-way signal attenuation.

Small millimeter wave antennas are often integrated on chip. During prototyping, the antenna can typically be accessed only using a probe station. However, traditional antenna measurement techniques have limitations in antenna on a probe station, for which the conventional methods are based on spherical measurement requiring complex mechanical arms for the probe antenna movements around the AUT [9–11].

The near-field wire-scattering technique presented in [12] might be suitable for antenna testing in a probe station. In this method, a thin wire is translated across the near-field of the AUT. A cut of the antenna pattern is solved from the measured reflection coefficients of the antenna at different wire positions. The method, however, is only capable to solve one pattern cut. In addition, an AUT with separable near-field distribution (total field can be represented as a product of field distribution in two orthogonal directions) is required.

In this paper, we present a novel antenna pattern retrieval method somewhat similar to the wire-scattering technique. In the proposed method, a reflective surface with known reflective properties is placed in the vicinity of the aperture of the AUT and the antenna reflection coefficient is measured. The measurement is repeated many times with different reflective surfaces. The antenna properties are solved from the measured reflection coefficients. The advantages of the method are that there are no flexing cables needed and the setup can be compact. In addition, the antenna near-field distribution does not need to be separable. The method in its current form can only solve a pattern cut, but in the future we aim at developing the method further such that antenna radiation pattern could be solved in 2D. Then the method could be feasible for characterizing antennas even in a probe station. The method is somewhat similar to the antenna RCS technique with an exception that instead of antenna feed, the antenna near-field is terminated with a modulating load.

2. PROPOSED ANTENNA PATTERN RETRIEVAL METHOD

In this method, a reflection coefficient of an antenna is measured when the antenna is placed close to a reflecting surface, whose reflection properties vary spatially in a known way. The measurement is repeated with different reflective surfaces, for example moving the reflective surface over the antenna between each measurement. After an adequate amount of information is gathered, the near-field distribution of the antenna is solved from the measured reflection coefficients and the known reflector properties. In the following, we equate the reflector properties to the antenna reflection coefficient and show how the antenna near-field distribution can be solved from a set of measurements.

For simplicity, we derive the theoretical basis for an antenna with planar aperture transmitting at one polarization. In addition, we restrict to a case, where the reflective surface is planar. However, it can be considered straightforward to extend the theory for non-planar aperture or reflective surface, and for arbitrary polarization.

2.1. Reflection Coefficient

Consider an antenna having an electrical aperture field distribution $E_{\mathrm{AUT}}(x, y, z)$ and assume that the ratio between electric and magnetic field is the free space wave impedance. The aperture is in parallel to a reflection plane, whose spatial reflection coefficient is given by $\Gamma(x, y)$. The reflection plane is offset from the aperture by z_0. Fig. 1 shows the schematic layout of the pattern retrieval process.

The field produced by the antenna on the plane $z = z_0$ can be calculated by representing the aperture field with plane wave components propagating into different directions, advancing all components by the offset distance z_0, and summing the plane waves back to the spatial domain. The field propagation could also be solved with alternative methods, for example using the Huygens' Principle. Using the plane wave approach, the plane wave spectrum of the antenna aperture field at $z = 0$ is

$$P_{\mathrm{AUT}}(k_x, k_y, z = 0) = \frac{1}{2\pi} \iint_S (E_{\mathrm{AUT}}(x, y, z = 0)) e^{j(k_x x + k_y y)} d_x d_y \tag{1}$$

where S is the aperture surface and k_x and k_y are the x- and y-components of the wave vector ($|\mathbf{k}| = k = 2\pi/\lambda$). For convenience, we define the operation of Eq. (1) as the inverse Fourier transform

and denote it with the symbol $\mathcal{F}^{-1}$ (as $P_{\text{AUT}} = \mathcal{F}^{-1}\{E_{\text{AUT}}\}$) in the following text.

The plane wave spectrum on the plane $z = z_0$ is given as

$$P_{\text{AUT}}(k_x, k_y, z = z_0) = P_{\text{AUT}}(k_x, k_y, z = 0) e^{-jk_z z_0} \tag{2}$$

where $k^2 = k_x^2 + k_y^2 + k_z^2$. The propagated field at point (x, y) on the plane $z = z_0$ is given in terms of the plane wave components as

$$E_{\text{AUT}}(x, y, z = z_0) = \frac{1}{2\pi} \int_{-k}^{k} \int_{-k}^{k} P_{\text{AUT}}(k_x, k_y, z = z_0) e^{-j(k_x x + k_y y)} dk_x dk_y \tag{3}$$

where the evanescent wave contribution is neglected under an assumption that the offset z_0 is large compared to the reactive near-field distance (sometimes approximated as $\lambda/2\pi$). Let the operation of Eq. (3) be defined as the Fourier transform ($E_{\text{AUT}} = \mathcal{F}\{P_{\text{AUT}}\}$).

The field given by Eq. (3) reflects from the reflective surface shown in Fig. 1 and then propagates back to the antenna. The reflected wave on the plane $z = 0$ is given as

$$E_{\Gamma}(x, y, z = 0) = \mathcal{F}\left\{ \mathcal{F}^{-1}\left\{ E_{\text{AUT}}(x, y, z = z_0) \Gamma(x, y) \right\} e^{-jk_z z_0} \right\} \tag{4}$$

where $\Gamma(x, y)$ is the spatial reflection coefficient of the surface. The reflection coefficient referenced to the aperture plane of a lossless and perfectly matched antenna due to the reflective load is given as

$$S_{11,\,\text{aperture}} = \frac{\iint_S E_{\Gamma}(x, y, z = 0) E_{\text{AUT}}(x, y, z = 0) \, dx dy}{\iint_S E_{\text{AUT}}(x, y, z = 0) E_{\text{AUT}}^*(x, y, z = 0) \, dx dy} \tag{5}$$

where $*$ denotes complex conjugate. When there is an impedance mismatch between the antenna and the generator or other environmental scatterers in addition to the intended load, the reflection coefficient contains a constant term $S_{11,\,\text{static}}$ that is assumed to be independent of the varying reflective load. For simplicity, possible multiple reflections between the AUT and environment are neglected. The reflection coefficient referenced to the antenna feed can be written as

$$S_{11} = S_{11,\,\text{static}} + e^{2(j\theta - \alpha)} S_{11,\,\text{aperture}} \tag{6}$$

where θ is the phase delay and α the attenuation constant between the antenna feed and aperture plane.

2.2. Solving Antenna Near-field Distribution

In this method, antenna reflection coefficient is measured multiple times such that the antenna is loaded with a unique reflective surface in each measurement. Then, an antenna aperture field that best explains the measurement results is iteratively solved using Eqs. (1)–(6). Note that it is adequate to sample the antenna aperture with $\lambda/2$-interval because z_0 is chosen to be so large that the evanescent modes can be neglected. In addition, the field can be spatially limited according to the physical aperture of the antenna.

It is possible to solve all the unknowns, $S_{11,\,\text{static}}$, θ, α, and E_{AUT} from the measurements. The reflective load independent term of the antenna reflection coefficient $S_{11,\,\text{static}}$ can be either found out by measuring the reflection coefficient of the antenna when the aperture is loaded with absorbing material $\Gamma(x, y) = 0$ or it can be solved as an unknown parameter. The iteration algorithm always try to find the best fit to the target (herein, reflection coefficient). The phase delay term can be embedded into the unknown antenna aperture field E_{AUT}, therefore, the aperture field is found out using the following least-squares fitting, i.e., minimizing Δ

$$\Delta = \min_{E_{\text{AUT}}, \alpha} \sum_n \left| S_{11,\,\text{aperture}}(E_{\text{AUT}}, \Gamma_n(x, y)) e^{-2\alpha} + S_{11,\,\text{static}} - S_{11,n} \right|^2 \tag{7}$$

where $S_{11,n}$ is the nth measured or simulated reflection coefficient and $\Gamma_n(x, y)$ the respective spatial reflection pattern of the reflective surface.

The least-squares cost function is the best estimator when the measured reflection coefficient is corrupted by additive white Gaussian noise. Although the validity of this condition is uncertain, the least-squares cost function is selected as an educated guess.

2.3. Practical Considerations

The model neglects the evanescent field modes in the propagation. Therefore, it is important to select the measurement geometry such that the evanescent modes generated by the AUT are weak enough at the reflective plane. To ensure this, the distance z_0 is chosen outside the reactive near-field region which for electrically large antennas is given as $z_0 \geq 0.62\sqrt{A^3/\lambda}$. Typically an antenna is considered to be electrically large if $A > \lambda$, where A is the antenna maximum dimension [13].

The angular region, from which far-field information is gathered, depends on the measurement geometry. Outside this valid angular region, the method is incapable to obtain correctly the far-field pattern. In the present case the valid angular region can be approximately derived from the geometry of the measurement setup and it is

$$\theta_{\text{valid}} = \tan^{-1}\left(\frac{D_{\text{move}} - A}{2z_0}\right) \tag{8}$$

where D_{move} denotes the total moving distance of the reflective surface (see the setup shown in Fig. 1).
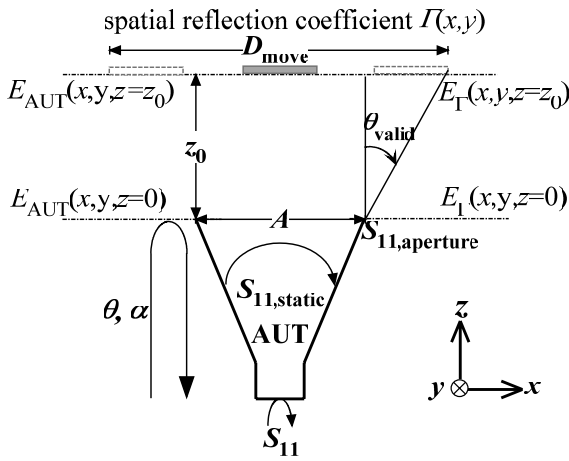

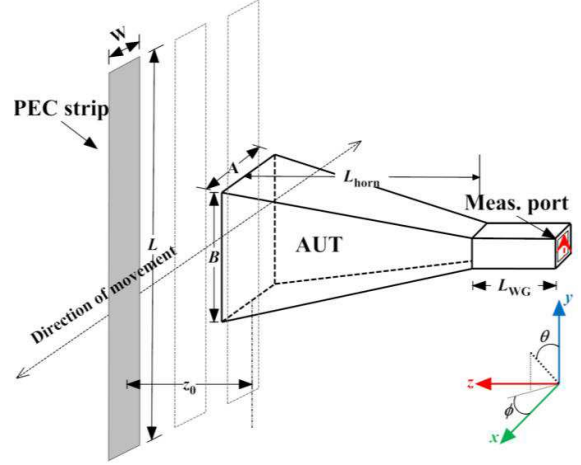**Figure 1.** Schematic layout of the proposed antenna pattern retrieval method.

Figure 2. Simulation setup and the pyramidal horn dimensions (not to scale).

3. SIMULATIONS AND EXPERIMENTS

The proposed method is tested experimentally and by simulations using a Ka-band pyramidal horn antenna operating at 30 GHz as the AUT. A vertical copper (PEC in simulation) strip is used as the reflector. It is placed at a distance of z_0 in front of the AUT. The coppers trip is horizontally moved along x-direction between every reflection coefficient measurement with a step of 5 mm ($\sim \lambda/2$). The width of the reflective strip is chosen to be less than the AUT aperture but large enough to provide

Table 1. Dimensions used in simulations and experiments (see Fig. 2 for reference).

Parameter	Value (mm)	Parameter	Value (mm)
W	25	L_{horn}	55.35
L	125	L_{WG}	15
A	37.85	z_0	60
B	28.45		

reflection. The height of the copper strip is three times that of the AUT aperture. The setups used in the experiments and simulations are shown in Figs. 2 and 4 with all the dimensions listed in Table 1. The same dimensions have been used both in experiments and in simulations. The thickness of the AUT wall and PEC strip used in simulations is 0.1 mm, while the thickness of the manufactured AUT wall and copper strip are 0.7 mm and 0.25 mm respectively.

3.1. Simulations

A model according to the schematic design is created using full-wave EM simulation software (Ansoft HFSS v15). The AUT is fixed at a particular position and it is excited by a wave port at the measuring terminal. Particularly, the electric field at the AUT aperture is exported as the original source field to verify the equations listed in Section 2 and as a reference for further comparison. Fig. 3 shows the comparison of the reflection coefficients calculated using the exported AUT aperture field with Eqs. (1)–(5) and those obtained directly from the simulator. A good agreement between the two reflection coefficients is observed.
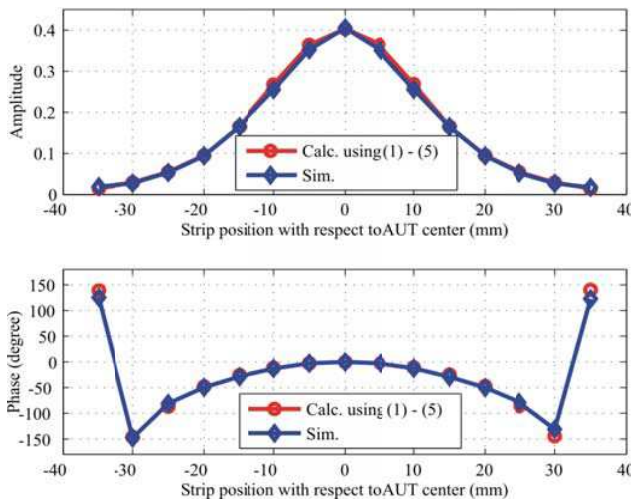

Figure 3. The comparison of reflection coefficient calculated using Eqs. (1)–(5) and obtained from simulator.
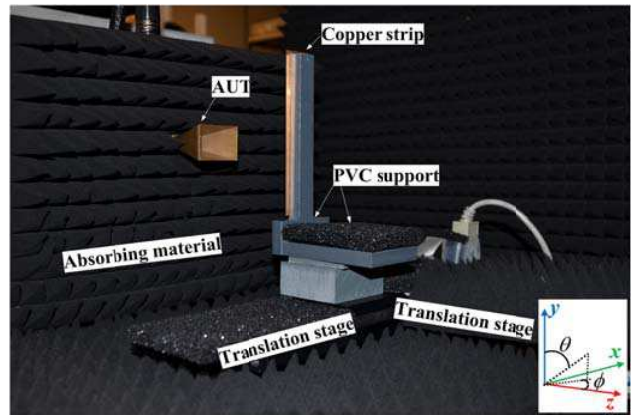

Figure 4. Photograph of the experimental setup.

3.2. Experimental Setup

Figure 4 shows the assembly of the experimental setup in which the AUT is fixed on a customized PVC-based holder covered with absorbing material. A copper strip is attached to the PVC support mounted on the linear translation stage which is controlled by a LabVIEW program. The reflection coefficient of the AUT is measured with a calibrated network analyzer (Agilent PNA E8363A) at each particular strip position. Because it was assumed that the multiple reflections between the copper strip and the AUT aperture could affect the measured S_{11}, the measurement is repeated at standard 60 mm distance and 57.5 mm ($\sim \lambda/4$ offset) respectively in order to cancel this effect. Note that multiple reflections between the reflective surface and AUT are not included in the analytical model. The radiation pattern of the AUT was also measured in a standard anechoic chamber in a far-field range for providing reference.

3.3. Solving the Aperture Field and Antenna Pattern

The aperture field is found out from the least-squares Eq. (7) in Section 2. Full reflection is assumed from the copper strip and zero reflection elsewhere, which is mathematically formulated as

$$\Gamma_n(x,y) = \begin{cases} -1, & \text{when } |x - x_{\text{offset}}| < \frac{W}{2} \text{ and } |y| < \frac{L}{2} \\ 0, & \text{elsewhere} \end{cases} \qquad (9)$$

where x_{offset} is the offset of the strip from its center position.

Due to the physical constraints, the aperture field is set to zero outside the physical horn opening and its vertical distribution is assumed to be independent of the horizontal coordinate. Eq. (7) is solved iteratively using the quasi-Newton method starting from the initial guess for the aperture near-field given as

$$E_{\text{AUT}}(x, y, z = 0) = \begin{cases} A_{\text{initial}} e^{j\theta_{\text{initial}}} & \text{when } |x| < \frac{A}{2} \text{ and } |y| < \frac{B}{2} \\ 0, & \text{elsewhere} \end{cases} \tag{10}$$

where A and B are the aperture dimensions of the horn as shown in Fig. 2, A_{initial} and θ_{initial} are the initial guess of the amplitude and phase respectively. Normally we choose values with uniform amplitude and phase and normalize this electric field distribution to unity,hence, $A_{\text{initial}} = 1$, $\theta_{\text{initial}} = 1$.

4. RESULTS AND DISCUSSIONS

Figure 5 depicts the amplitude and relative phase of the simulated and measured antenna reflection coefficient as a function of the strip position respectively. Note that the reflection coefficients are without the corresponding reflective load independent term. The measured and simulated results are in good agreement. The measured reflection coefficient is slightly asymmetric with respect to the strip position, whereas the simulated one is not. This is likely due to a small misalignment of the strip.

The simulated and measured reflection coefficients were used to solve the antenna near-field distribution from Eq. (7). The near-field electrical distributions obtained from the simulated and measured S_{11} are shown in Fig. 6. The near-field distributions calculated from the measured far-field pattern and directly from the simulator are shown as well for reference. The calculated relative near-field phase distributions within the AUT physical aperture agrees reasonably well to the simulated and measured results. Note that the method is capable for solving the antenna far-field pattern only in the valid angular region given in Eq. (8). The measured and simulated near-field distributions, however, contain also wave modes radiating outside the valid angular region. Therefore, the true near-field distribution of the antenna should not be exactly the same as that obtained with the method, provided that the valid angular range is smaller than the visible spectrum.

The reconstructed reflection coefficient using the solved near-field distribution is also shown in Fig. 5, in which both the amplitude and phase are in good agreement. This indicates that the fitting process may converge in the minimum under certain circumstances. Fig. 7 shows the comparison of the reconstructed, simulated and measured normalized radiation patterns at 30 GHz. The results are in good agreement between $-25° \ldots 25°$ which is the calculated valid angular region with the physical dimensions of the current setup. The reconstructed pattern with the measured S_{11} deviates less than 0.5 dB from the measured pattern at -16 dB level.

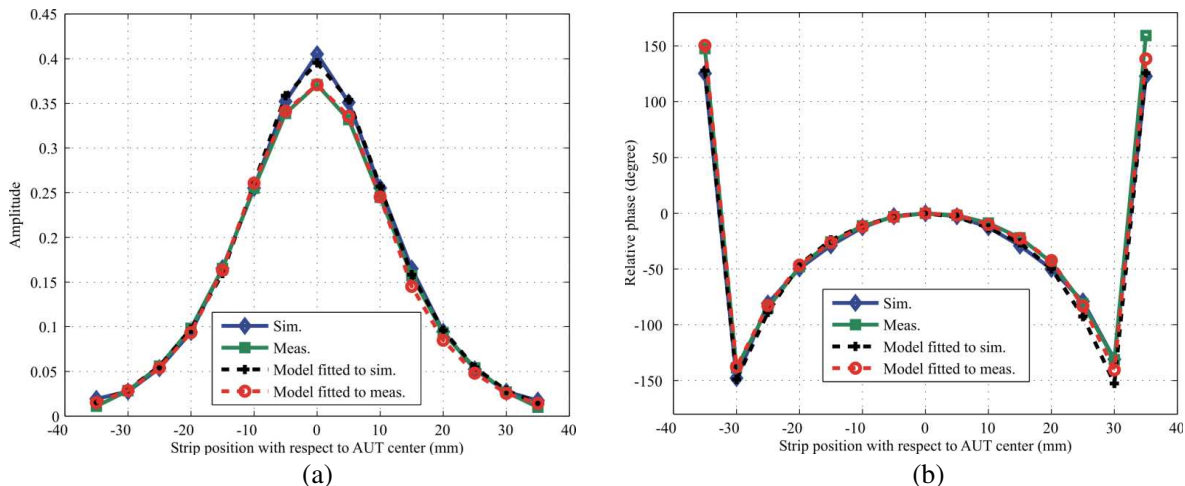These results show that the proposed method is suitable for characterizing certain types of antennas

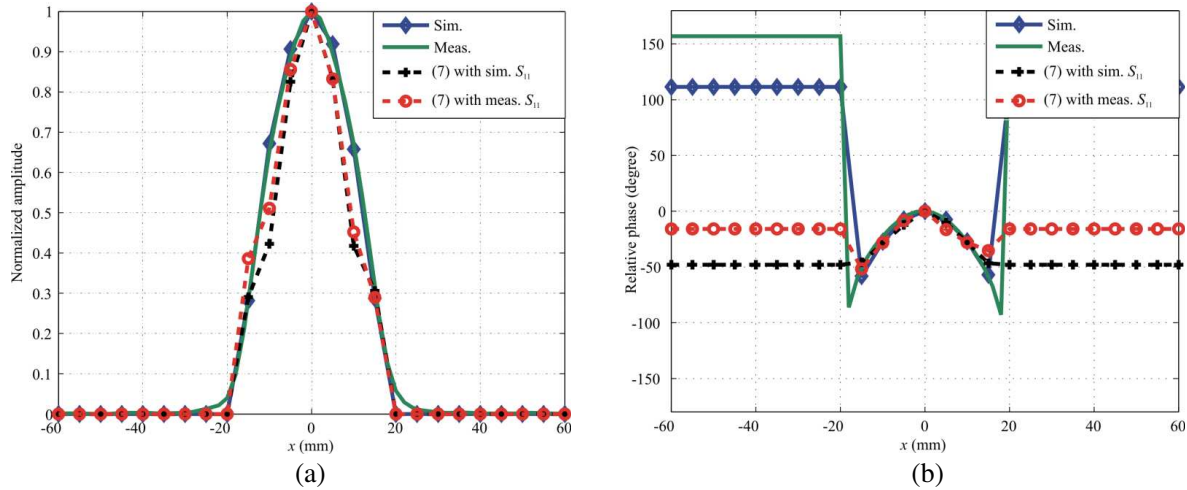**Figure 5.** Simulated and measured S_{11}: (a) amplitude; (b) relative phase.

Figure 6. Electric near-field distribution at AUT aperture: (a) normalized amplitude; (b) relative phase.
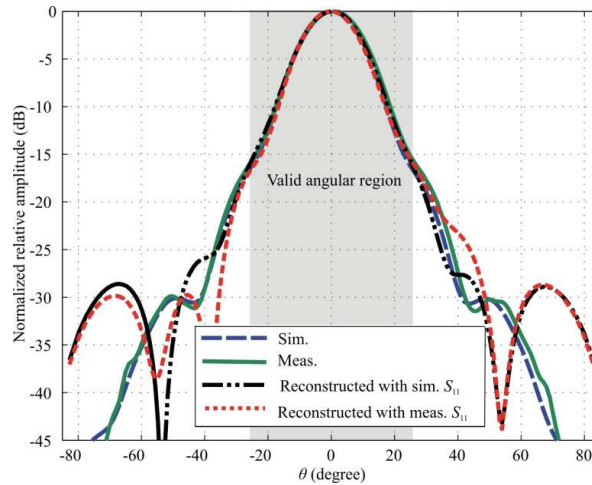

Figure 7. Normalized far-field pattern at 30 GHz.

without a need for a traditional two-way measurement. It might also be possible to extend the current method to 2D aperture antennas and other polarizations with the variation of a proper reflective surface in a 2D plane and polarization-sensitive reflective surface. There is also a possibility to extend this method to characterize small antennas on a probe station if the reflective surface can be scaled down in size.

The measurement accuracy provided already by these initial results seems adequate for certain purposes. It is likely that the method could be further improved by introducing another cost function for fitting and maybe finding other fitting algorithms. In addition, neither the measurement geometry nor the reflective plane has been optimized. Another selection of these might lead into a better accuracy and another valid angular region.

The primary aim of this paper is to derive and verify the equations relating the properties of the reflective load to the measured reflection coefficient. The paper also demonstrates that the antenna pattern can be solved with the method. Further improvement of the inversion method and optimization of the reflective surface are left for a topic of future research.

5. CONCLUSION

A new antenna pattern retrieval method is proposed. In this method, the antenna reflection coefficient is measured many times when a unique reflective load with known spatial reflection properties is placed near the antenna in each measurement. The antenna pattern is obtained from the measurements with

an inversion algorithm. This paper presents analytical equations for equating the antenna reflection coefficient to the near-field load of the antenna. Simulations were used to verify the theoretical basis and the method was experimentally demonstrated at 30 GHz. The results show that the method could enable sufficient accuracy with low gain antennas or in the vicinity of main lobe with directive antennas.

ACKNOWLEDGMENT

REFERENCES

1. Karttunen, A., J. Ala-Laurinaho, M. Vaaja, T. Koskinen, J. Häkli, A. Lönnqvist, J. Mallat, A. Tamminen, V. Viikari, and A. V. Räisänen, "Antenna tests with a hologram-based CATR at 650 GHz," *IEEE Transactions on Antennas and Propagation*, Vol. 57, No. 3, 711–720, Mar. 2009.

2. Häkli, J., T. Koskinen, A. Lönnqvist, J. Säily, J. Mallat, J. Ala-Laurinaho, V. Viikari, J. Tuovinen, and A. V. Räisänen, "Testing of a 1.5 m reflector antenna at 322 GHz in a CATR based on a hologram," *IEEE Transactions on Antennas and Propagation*, Vol. 53, No. 10, 3142–3150, Oct. 2005.

3. Lönnqvist, A., T. Koskinen, J. Häkli, J. Säily, J. Ala-Laurinaho, J. Mallat, V. Viikari, J. Tuovinen, and A. V. Räisänen, "Hologram-based compact range for submillimeter-wave antenna testing," *IEEE Transactions on Antennas and Propagation*, Vol. 53, No. 10, 3151–3159, Oct. 2005.

4. Säily, J., P. Eskelinen, and A. V. Räisänen, "Pilot signal-based real-time measurement and correction of phase errors caused by microwave cable flexing in planar near-field tests," *IEEE Transactions on Antennas and Propagation*, Vol. 51, No. 2, 195–200, Feb. 2003.

5. King, D. D., "The measurement and interpretation of antenna scattering," *Proceedings of the IRE*, Vol. 37, No. 7, 770–777, Jul. 1949.

6. Wiesbeck, W. and E. Heidrich, "Wide-band multiport antenna characterization by polarimetric RCS measurements," *IEEE Transactions on Antennas and Propagation*, Vol. 46, No. 3, 341–350, Mar. 1998.

7. Appel-Hansen, J., "Accurate determination of gain and radiation patterns by radar cross-section measurements," *IEEE Transactions on Antennas and Propagation*, Vol. 27, No. 5, 640–646, Sep. 1979.

8. Pursula, P., M. Hirvonen, K. Jaakkola, and T. Varpula, "Antenna effective aperture measurement with backscattering modulation," *IEEE Transactions on Antennas and Propagation*, Vol. 55, No. 10, 2836–2843, Oct. 2007.

9. Ranvier, S., M. Kyrö, C. Icheln, C. Luxey, R. Staraj, and P. Vainikainen, "Compact 3-D on-wafer radiation pattern measurement system for 60 GHz antennas," *Microwave and Optical Technology Letters*, Vol. 51, No. 2, 319–324, Feb. 2009.

10. Beer, S. and T. Zwick, "Probe based radiation pattern measurements for highly integrated millimeter-wave antennas," *Proceeding of 4th European Conference on Antennas and Propagation*, 1–5, Apr. 2010.

11. Mohammadpour-Aghdam, K., S. Brebel, A. Enayati, R. Faraji-Dana, G. A. E. Vandenbosch, and W. Deraedt, "RF probe influence study in millimeter-wave antenna pattern measurements," *International Journal of RF and Microwave Computer-Aided Engineering*, Vol. 21, No. 4, 413–420, Jul. 2011.

12. Calazans, T., H. D. Griffiths, A. L. Cullen, D. E. N. Davies, and R. Benjamin, "Antenna radiation pattern measurement using a near-field wire scattering technique," *IEE Proceedings — Microwaves, Antennas and Propagation*, Vol. 145, No. 3, 263–267, Jun. 1998.

13. Balanis, C. A., *Antenna Theory: Analysis and Design*, 3rd edition, Wiley, 2005.